IEEE Robotics and Automation Letters (RA-L) paper, presented at ICRA 2026, Vienna, Austria. Cite as RA-L paper.

Robust and Error-Tolerant Peg-in-Hole Assembly Using Simple Control

Masanori Ueda[1], Tokuo Tsuji[2], Shota Ishikawa[1 3], Tatsuhiro Hiramitsu[2], Hiroaki Seki[2], Yosuke Suzuki[2], Toshihiro Nishimura[2] and Tetsuyou Watanabe[2]

***Abstract*— We developed a simple peg-in-hole strategy that uses flexible joints and peg rotations. Even when the circle peg in the peg-in-hole assembly contains position and orientation errors, it can be inserted in a passive and robust manner. Additionally, using force-torque sensors to estimate the contact position allows the correction of the orientation of the peg and its insertion into the hole if the initial attempt fails. We conducted horizontal and vertical peg-in-hole experiments with random position and orientation errors to demonstrate the effectiveness of the developed method. This method does not rely on high-frequency sensors or servos, which enables a quick and low-cost peg-in-hole assembly with tolerance to position and orientation errors and direction.**

I. INTRODUCTION

Peg-in-hole assembly is a fundamental operation in robotic assembly tasks that requires robots to precisely insert an object into a target hole. Therefore, peg-in-hole tasks require high-precision alignment of the positions and orientations of the object and hole, making them challenging to automate. By accomplishing this task, automation can be implemented not only in production lines that require peg-in-holes such as electronic devices [1] and assembly engines [2], but also in other assembly operations from the perspective of aligning parts and holes. Circular peg-in-hole assembly tasks are commonly observed in many industrial products such as engine assembly [2] and bearing insertion [3]. Currently, work is performed on faces using jigs and precise teaching. However, this approach lacks robustness [4]. Therefore, research is being conducted on automated peg-in-hole methods that use sensing technology and advanced controls. Methods that primarily use force and vision sensors have been proposed for peg-in-hole sensing. For example, methods using force sensors analyze forces and torques on contact or use machine learning to estimate the contact state and decide how to move next. A guide map was developed by Newman *et al.* [5] from force-torque data at the contact point between the peg and hole surface, and the contact state and position estimation of the hole were achieved by analyzing the force-torque sensor [6]–[8]. Methods using vision sensors have also been explored [9]. For example, image-based visual servo systems [10] that extract features and minimize discrepancies and position-based visual servo systems [11], which estimate the position and orientation of an object in a peg-in-hole assembly within the coordinate system of a camera have been developed. Recently, machine learning methods have been introduced in addition to analytical techniques [12]–[14]. In these methods, robot control is achieved using feedback from the force and vision sensors to perform peg-in-hole tasks.

As the clearance between the peg and hole in a peg-in-hole assembly decreases, a higher precision is required, which increases the cost and necessitates higher-frequency sensors. Additionally, vision sensors require calibration and may experience reduced accuracy owing to changes in the environment or the objects observed. Therefore, sensorless automation methods for peg-in-hole tasks have been investigated. Dual peg-in-hole operations in which two or more pegs are inserted simultaneously, have been achieved without sensors under environmental constraints [15]. Furthermore,

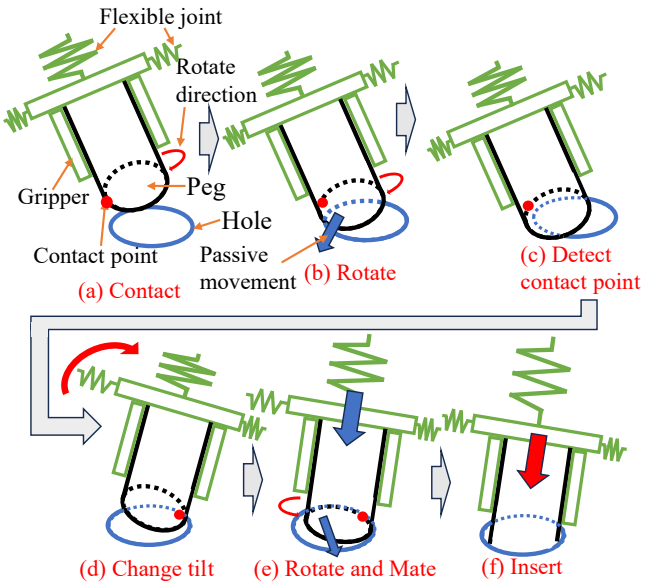

Fig. 1: An overview of our method. When the gripper with a flexible joint grasps and presses the peg (a), the peg rotates and moves about the point of contact (b). If the peg does not enter the hole when it moves, then the contact point is estimated (c) and the peg is tilted in the opposite direction (d). The stored pushing force in the flexible joints is released when the peg and the hole are nearly aligned, thereby allowing the peg to slip into the hole (e).

[1] M. Ueda and S. Ishikawa are students of Graduate School of Natural Science and Technology, Kanazawa University, Kakuma-machi, Kanazawa-shi, Ishikawa, 920-1192, Japan. masanoriueda0317, i2424122001@stu.kanazawa-u.ac.jp

[2] T. Tsuji, T. Hiramitsu, H. Seki, Y. Suzuki, T. Nishimura, and T. Watanabe are with Faculty of Frontier Engineering, Institute of Science and Engineering, Kanazawa University, Kakuma-machi, Kanazawa-shi, Ishikawa 920-1192, Japan. tokuo-tsuji, thiramitsu, hseki, suzuki, tnishimura, twata@se.kanazawa-u.ac.jp

[3] S. Ishikawa is with DENSO CORPORATION, 500-1 Minamiyama, Komenoki-cho, Nisshin, Aichi, 470-0111, Japan. shota.ishikawa.j8m@jp.denso.com

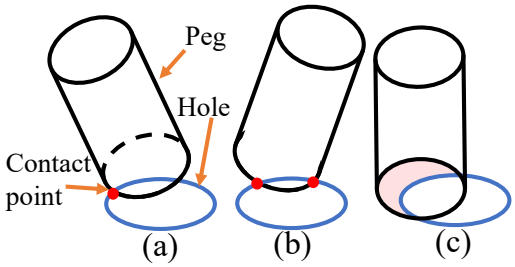

Fig. 2: Contact states between the peg and hole during peg-in-hole failures: (a) single-point contact, (b) two-point contact, and (c) surface contact.

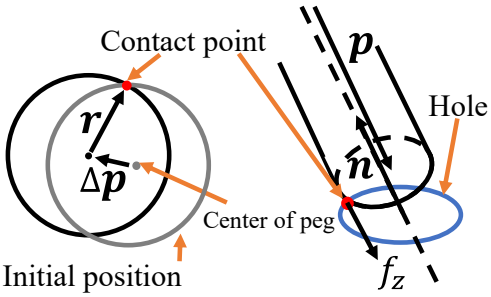

Fig. 3: Single-point contact state: pushing force F_z applied to the peg, rotation axis vector $\boldsymbol{n}$, position vector $\boldsymbol{r}$ from the center of the peg to the contact point, movement vector $\boldsymbol{\Delta p}$ from its initial position, and position vector $\boldsymbol{p}$ from the joint to the bottom of the peg.

methods that control robots to achieve virtual compliance and enhance exploration efficiency were proposed. Research achieved single-peg-in-hole tasks based on encoders by applying active compliance control to guide a peg around a hole [16]. This method was inspired by the fact that humans can insert an object without knowing the precise location of a hole, and they can efficiently search for a hole by tracing a spiral trajectory. However, active compliance control requires complex robot controllers, and high resolution leads to long search times. In these methods, the use of high-precision and high-frequency sensors and servos improves the accuracy and speed of operations. However, challenges include the calibration of cameras or robots, responding to changes in the environment and objects [4], and complex robot controllers [17].

In contrast, passive compliance control, which involves the installation of flexible mechanisms on robot arms, can be implemented easily without complex controls, high-performance actuators, or sensors [18]–[20]. It can perform robust assembly operations because it can easily adapt to object changes. In our previous study, we developed a method called Contact and Rotation (CaR) to achieve a peg-in-hole assembly by rotating the peg using a flexible mechanism [20]–[22]. This method only requires rotation of the peg for alignment to achieve a peg-in-hole assembly, which requires a rotational mechanism on the gripper while

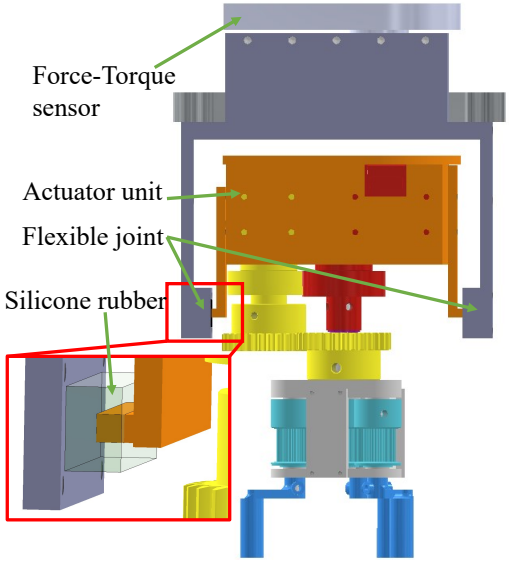

Fig. 4: Gripper equipped with flexible joints and the infinity rotatable function is used in this study.

eliminating the need to control the robot arm. To address these challenges, we propose a simple and rapid circular peg-in-hole method using a passive compliance system. This is achieved by the peg moving around the contact point through its own rotation, exploring while the flexible mechanism allows its motion within the range of motion. This method achieves high-speed peg-in-hole operation without requiring high-frequency sensors, servos, or complex robot controllers for the control actions of exploration. In this study, we performed a mechanical analysis of this technique and determined the conditions for performing peg-in-hole tasks by rotating a circular peg. Subsequently, using a force sensor, we obtained the contact state of the peg at the time of failure and developed a method to expand the allowable range of positional and orientational errors by altering that state. The contact point was estimated from the change in momentum caused by the peg transfer. By tilting the gripper in the direction opposite to the contact point during insertion, the system becomes more robust against errors in position and orientation. Furthermore, this method was confirmed to be effective for horizontal peg-in-hole tasks.

II. Rotation Based Strategy for Peg-in-Hole Tasks

An overview of the CaR and orientation correction strategies is shown in Fig. 1. In the CaR method, the movement of the circular peg in a peg-in-hole task is facilitated by friction and rotation within the flexible range of the joints of the gripper. The gripper, which is equipped with flexible joints, grasps the peg and begins to insert it into the hole. If a position error exists between the hole and peg, insertion may fail, thereby causing the peg to press against the edge of the hole. When the peg is rotated, it begins to pivot around the contact point of the hole. As the peg and the hole become nearly aligned, the flexible joints release the pressing force,

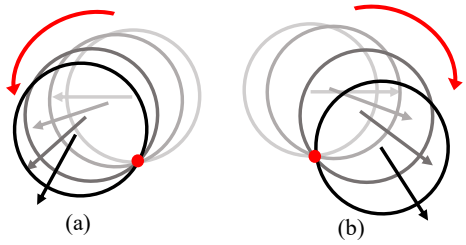

Fig. 5: Trajectory of the peg when rotating (a) counterclockwise and (b) clockwise. The movement direction varies with the rotation direction.

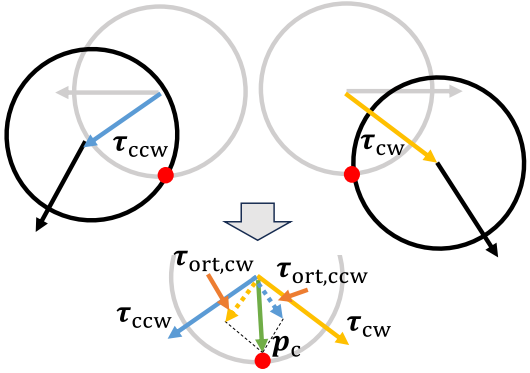

Fig. 6: Estimating the contact direction vector $\boldsymbol{p}_c$ by averaging the orthogonal components $\boldsymbol{\tau}_{ort,ccw}$ and $\boldsymbol{\tau}_{ort,cw}$ of the moment vectors during both counterclockwise $\boldsymbol{\tau}_{ccw}$ and clockwise $\boldsymbol{\tau}_{cw}$ rotations of the peg.

thereby allowing the peg to slide into the hole. This strategy enables peg-in-hole insertion even in the presence of position errors. However, as shown in Fig. 2(c), the peg does not move significantly when in contact with the hole surface. Thus, in this study, we detected the contact point and changed the orientation in the opposite direction to achieve the state shown in Fig. 2(a) or Fig. 2(b), thereby including cases in which the peg did not enter the hole with just one rotation.

A. Flexible Joint and Gripper

In this study, we use a gripper with an infinite rotation mechanism of the palm and a flexible joint as previously developed [22]. The infinite rotation mechanism allows peg rotation and also screw turning, making it a versatile gripper. The flexible joint is structured as shown in Fig. 4. Protrusions extending from the left and right sides of the actuator unit were inserted into the recesses of the silicone rubber. Therefore, this flexible joint exhibits six degrees of freedom in flexibility. The flexible joints are located at the center of gravity of the actuator part. The distance from the force sensor of this gripper to the flexible joint is 95.7 mm, and the distance from the flexible joint to the palm is 55.7 mm. The force and torque acting on the force sensor are converted into the force and torque in the flexible joints using this value.

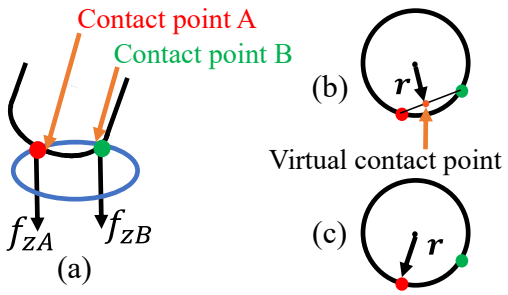

Fig. 7: (a) Two-point contact scenario: contact point A experiences compressive force F_{zA} and contact point B experiences F_{zB}. (b) The equilibrium point between A and B is treated as a virtual contact point. (c) When the static friction at point B is less than the force applied to the peg.

The stiffness matrix $\boldsymbol{K}$ of this flexible joint is as follows:

$$\boldsymbol{K} = \mathrm{diag}(k_{fx}, k_{fy}, k_{fz}, k_{mx}, k_{my}, k_{mz})$$

where, k_{fx}, k_{fy} and k_{fz} denote the stiffnesses in the x, y, and z directions, respectively; and k_{mx}, k_{my} and k_{mz} denote the rotational stiffnesses in the x, y, and z directions, respectively. The units are N/mm and N/rad. Based on the results of the flexibility experiments with the flexible joints [22], the stiffness values are set as follows: k_{fx} = 3.62 N/mm, k_{fy} = 0.828 N/mm, k_{fz} = 7.15 N/mm, k_{mx} = 1.84 Nm/rad, k_{my} = 6.00 Nm/rad and k_{mz} = 3.41 Nm/rad.

B. Analysis of CaR

Without the application of the CaR strategy, if the peg insertion fails, as shown in Fig. 2, the following three types of contact states can occur between the peg and hole:

(a) Single-point contact
(b) Two-point contact
(c) Surface contact

In this study, we first analyzed the single-point contact case, as shown in Fig. 3. We define the pressing force f_z, rotational axis vector $\boldsymbol{n}$, rotational torque τ, position vector $\boldsymbol{r}$ from the center of the peg to the contact point, position vector from the flexible joint to the bottom of the peg $\boldsymbol{p}$, and movement vector $\boldsymbol{\Delta p}$ of the peg from the initial position. Let the stiffness matrix of the flexible joint be $\boldsymbol{K}$ and the static friction coefficient between the peg and the hole be μ. When the peg rotates around its axis, the forces acting on the contact point are as follows: 1. Static friction force f_{sf} between the peg and hole; 2. force $\boldsymbol{f_r}$ due to the rotational torque of the peg; and 3. elastic force $\boldsymbol{f_k}$ from flexible joints. If the static friction force f_{sf} exceeds the sum of the rotational force $\boldsymbol{f_r}$ and the elastic force $\boldsymbol{f_k}$, the peg rotates around the contact point without moving the contact point. The conditions for this rotation are expressed as follows:

$$f_{\mathrm{sf}} > |\boldsymbol{f_r} + \boldsymbol{f_k}| \tag{1}$$

The static friction force (f_{sf}), force due to rotation (f_r), and elastic force (f_k) are expressed as follows:

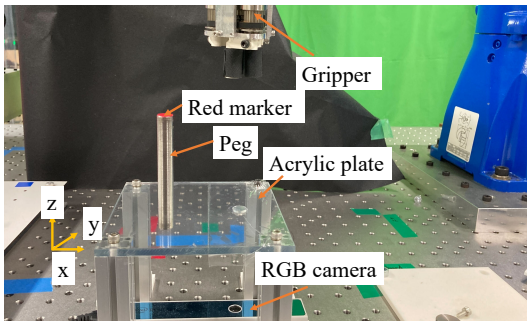

Fig. 8: Demonstration of the analysis experiment: A 10-mm-diameter peg with a red tip is used, and a camera is placed beneath a 10.2-mm-diameter hole on an acrylic board.

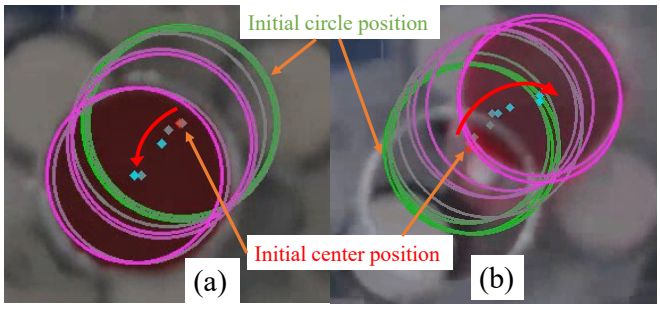

Fig. 9: Red dots denote the previous center of the peg; green circles show its previous positions. As it moves, the green circle changes to purple, and the red dot changes to light blue. (a) Clockwise rotation. (b) Counterclockwise rotation.

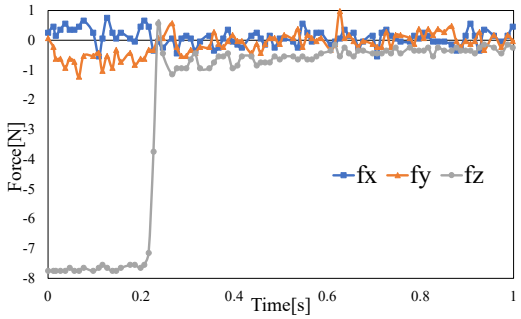

Fig. 10: Force sensor readings during peg-hole alignment during clockwise rotation. The force spikes when the peg slips into the hole.

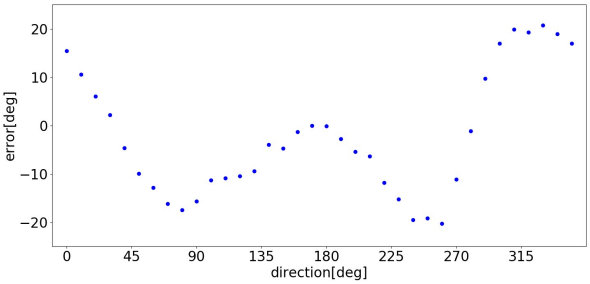

Fig. 11: Estimation of contact points by force sensation values. Tilt by 5° in directions from 0° to 360° in 10° increments, press at 20N and conduct experiments, showing the error between the predicted and actual values on the vertical axis and the direction on the horizontal axis.

$$f_{\mathrm{sf}} = \mu f_z \tag{2}$$

$$\boldsymbol{f_r} = \frac{\boldsymbol{n} \times \boldsymbol{r}}{|\boldsymbol{r}|^2}\tau \tag{3}$$

The elastic force (f_k) from the flexible joint is decomposed into the translational force (f_{k_f}) and the rotational force (f_{k_m}).

$$\boldsymbol{f_{k_f}} = \boldsymbol{K_f \Delta p} \tag{4}$$

$$\boldsymbol{f_{k_m}} = \frac{\boldsymbol{K_m}(\boldsymbol{p} \times \boldsymbol{\Delta p})}{|\boldsymbol{p}|^2} \tag{5}$$

where, $\boldsymbol{K_f}$ and $\boldsymbol{K_m}$ denote stiffness matrices of the flexible joint in the translational and rotational directions, respectively.

In the flexible joints used in this analysis, the stiffness term of the moment is lower than that of the force. Thus, when the same force is applied, the change due to the moment is greater. Therefore, in this analysis, we only consider the change in moments. By substituting (2)-(5) into (1), we obtain the following condition for the rotation about the contact point:

$$\mu f_z > |\frac{\boldsymbol{n} \times \boldsymbol{r}}{|\boldsymbol{r}|^2}\tau + \boldsymbol{K_f \Delta p} + \frac{\boldsymbol{K_m}(\boldsymbol{p} \times \boldsymbol{\Delta p})}{|\boldsymbol{p}|^2}| \tag{6}$$

According to Eq. (6), increases in the contact force enhances the ability of the peg to rotate around the contact point by exceeding the combined effects of the rotational torque and the elastic force. Although increases in the rotational speed reduces the search time, it requires a greater contact force. When (6) is satisfied, the force resulting from the rotational torque minus the elastic force acts on the center of the peg, his causes it to trace a trajectory, as shown in Fig. 5. This trajectory varies based on the rotation direction of the peg.

C. Contact Position Estimation Using the Peg Movement and Contact State Changes

As the peg moves in the CaR strategy, the force and moment measured by the force-torque sensor change. Given that the peg moves around a flexible joint, the moment changes are more significant than the force changes.

We estimated the position of the contact point by examining the moment vectors before and after the motion and considering the rotation direction of the peg. When the peg is rotated counterclockwise, it moves counterclockwise around the contact point. Thus, during the counterclockwise rotation, the contact point is inferred to be on the left side of the moment vector, whereas during clockwise rotation, it is on the right side.

By obtaining the moment vectors during both the counterclockwise and clockwise rotations, we estimated the position

of the contact point by averaging the orthogonal vectors. This is shown in Fig. 6. Estimating the position of the contact point leads to the adjustment of the position and orientation of the peg, achieving insertion over a wider range, even if the initial attempts fail. However, given that the hole and peg must remain in continuous point contact, polygonal pegs are not suitable for this analysis and estimation of the contact point.

D. Other Contact States and Transition to Single-Point Contact

Although our analysis focused on single-point contact, it is important to consider the two-point and surface-contact cases. In the surface contact scenario, the center of gravity of the contact area is considered as a virtual contact point around which the peg rotates. The distance between the contact point and the center of the peg is lower than that of the others, thereby reducing the search range due to the rotation of the peg. By performing the contact point estimation and posture change described in the previous section and changing to a single-point contact, it is possible to achieve peg-in-hole from a surface contact state.

The two-point contact state is shown in Fig. 7(a). Pressing forces f_{zA} and f_{zB} act at contact points A and B, respectively. As shown in Fig. 7(b), in the two-point contact case, the balance point between the contact points A and B acts as a virtual contact point, and the peg is assumed to rotate around this point. However, as shown in Fig. 7(c), if the static friction force at the contact point is lower than the sum of the rotational and the elastic forces, the point begins to slide and is ignored in the analysis. In the case of a two-point contact, the position of the contact points changes with the motion centered on the virtual contact point, transitioning to a one-point contact during the rotation.

III. Experiments

We conducted peg-in-hole experiments incorporating position and orientation errors using the CaR method and a simplified contact-position estimation method to verify its effectiveness. A Leptrino force-torque sensor (model FFS055YS102U6_S055F103) with a sampling frequency of 10 ms and a YASKAWA MOTOMAN-GP7 robot arm were used. The flexible-jointed gripper described in Section II-A was attached to the tip of the robot. The flexible joints allow the peg to move while the infinite rotation mechanism enables the peg to rotate continuously.

A. Experiment of Peg Trajectory

	diameter	contact force	tilting angle	error(result)
1	16 mm	20 N	5°	11.1°
2	16 mm	10 N	5°	18.9°
3	40 mm	20 N	5°	8.70°
4	16 mm	20 N	10°	6.49°

TABLE I: Results of the contact point estimation experiment with variations in contact force, peg diameter, and tilting angle.

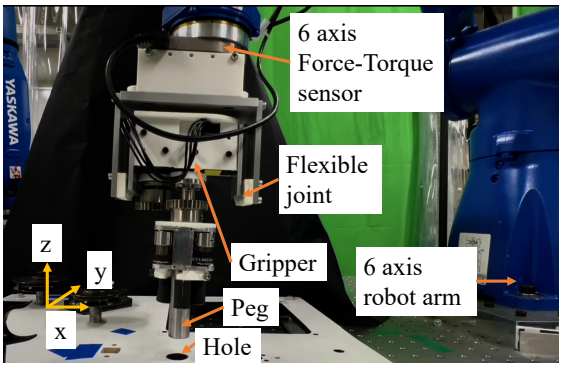

Fig. 12: Experimental setup for contact-position estimation and a peg-in-hole task with random position and orientation errors: A six-degree-of-freedom robot arm equipped with a force sensor and a gripper with flexible joints grasps a 16-mm-diameter peg. The clearance with the hole is 0.1 mm. The position errors are within an 8 mm^2 range, and the orientation errors varied randomly within an inverted cone centered at the base of the peg with a maximum tilt angle of 5°.

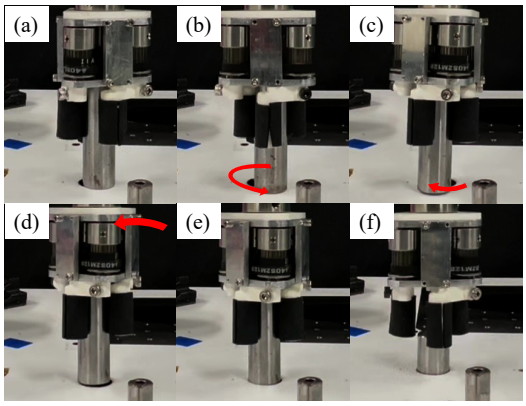

Fig. 13: Experimental progress. Perform CaR counter-clockwise and then clockwise and make posture corrections if it fails.

Based on the CaR analysis, we conducted an experiment to rotate a peg in contact with a hole, and the results confirmed that it moved around the contact point. As shown in Fig. 8, a peg with a red bottom is tilted at an angle of 5° and pressed against the edge of a hole in a perforated acrylic board. After rotating the peg, we confirm its movement trajectories by detecting the red area using a camera positioned below.

The experimental results are shown in Fig. 9. The green circles indicate the past positions of the peg, and the red dots represent the center of the peg at these times. The trajectory shows that the intersections of the green circles, which represent the centers of peg rotation, coincide with the holes. This indicated that the peg rotated around the contact point with the hole.

When the peg was rotated clockwise, as shown in Fig. 9(a), it moved around the contact point and approached the hole. When the peg and hole positions nearly coincide, the

pressing force stored in the flexible joint is released, and the peg slides into the hole. Conversely, when the peg is rotated counterclockwise, as shown in Fig. 9(b), it moves away from the hole.

This causes it to slip given that the sum of the rotational force $\boldsymbol{f_r}$ and elastic force $\boldsymbol{f_k}$ exceeding the static friction force and move to a new contact point. The force sensor readings during clockwise rotation of the peg are shown in Fig. 10. When the peg approximately aligns with the hole, at 0.2 s, force f_z in the pressing direction decreases sharply and approaches the force level of the free state. This observation allowed the alignment to be determined via monitoring the force in the pressing direction.

B. Experiment of Contact-Position Estimation

To verify the contact position estimation method described in Section II-C, an experiment was conducted to estimate the contact point using values of the force-torque sensors. A 16-mm-diameter peg was held and tilted at 5° in directions ranging from 0° to 360° in increments of 10°. Subsequently, the peg is pressed against the floor with 20 N to estimate the contact point. The experiment was conducted five times, and the results are shown in Fig. 11.

The mean absolute error from the true value was 11.1°and the standard deviation was 6.50°. The results of the experiment exhibited sufficient accuracy when estimating the contact point in the case of peg-in-hole failure and tilting in the opposite direction for correction. In addition, the results confirmed that the diameter of the peg or increases in the peg inclination angle improves accuracy. The results of experiments conducted by varying the peg size, contact force, and inclination angle are listed in Table. I. Increases in the tilt angle of the peg prevented surface contact, and increases in the contact force enhanced the friction of the peg, thereby reducing its slipperiness. In addition, a larger-diameter peg applies a greater rotational force, which facilitates a more accurate estimations of the contact points.

C. Peg-in-Hole Experiments with Position and Orientation Errors

The experimental setup is shown in Fig. 12. The peg used was a cylinder with a diameter of 16 mm and a length of 50 mm, which offered a clearance of 0.1 mm with the hole and did not contain a chamfer.

In the experiment, the gripper grasped the peg, and prior to insertion into the hole, a random positional error was introduced within an 8 mm^2 area centered above the hole. Introducing an orientation error of the peg involves tilting it in a random direction within the x-y plane. The tilt direction is defined by the azimuth angle θ, which ranges from 0° to 360°, and the inclination angle ϕ, which defines the tilt from the vertical z axis, ranging from 0° to 5°. This setup allows the peg to tilt randomly within an inverted conical boundary with the base of the peg as the apex, which effectively converts the tilt into rotation around the x- and y-axes.

After applying the position and orientation errors, we measured the z-direction force f_{free} in the non-contact state. The

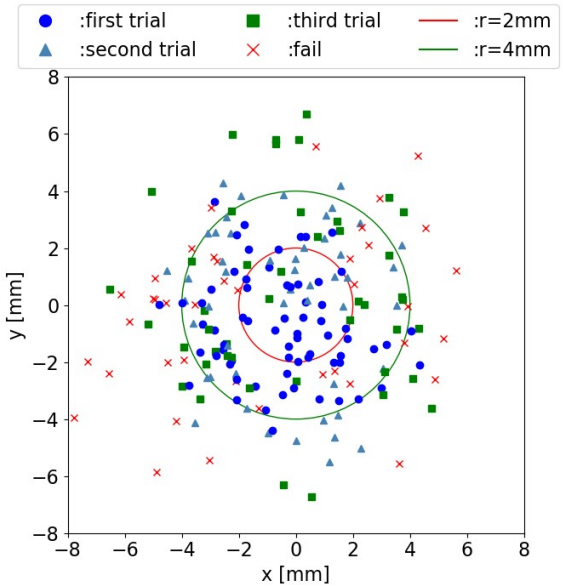

Fig. 14: Vertical peg-in-hole experimental results based on the top position of the peg: The horizontal axis denotes the x-axis position; the vertical axis denotes the y-axis position (mm). The success rate decreases with increases in the position error. The red circle has a radius of 2.0 mm, and the green circle has a radius of 4.0 mm. The success rate within each circle's range corresponded to 100% and 88.9%, respectively.

pegs were pressed using a contact force f_z of 10 N. The CaR method was used by first rotating the peg counterclockwise and then clockwise. If the difference between the force sensor reading in the pressing direction and f_{free} was 1 N or less, the peg was inserted while rotating, which was considered successful. If successful insertion was not achieved after the clockwise rotation, it was considered a failure.

In the method described in Section II-C, the contact position is estimated using the moments measured during counterclockwise and clockwise rotations, which require only slight rotational movements. Significant movements for exploration can increase the elastic forces and the shift contact points. To avoid increases in the execution time associated with the additional detection algorithms, we employed a simplified method.

The movement direction vector was calculated from the moments around the x- and y-axes during the initial counterclockwise rotation. Given that the contact position during counterclockwise rotation was on the left side of the movement direction, we obtained a vector orthogonal to the counterclockwise direction to serve as the contact direction vector. The moments used corresponded to those at the contact point and 0.1 s after the start of rotation. The gripper was then tilted 3° opposite to the contact direction vector to correct the orientation. This value was obtained under the same conditions as those used in the main experiment, as a preliminary experiment, and the success rates at each inclination without angle correction were compared. The

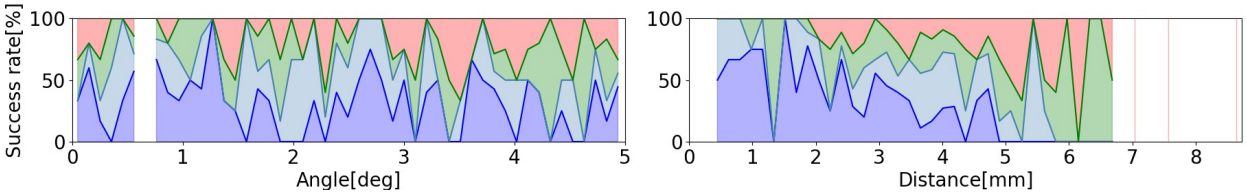

Fig. 15: Distribution of success rates based on the inclination angle and distance from the center. The left figure shows the inclination angle, and the right figure shows the distance from the center. The areas painted blue, light blue, and green indicate first, second, and third successes, respectively, while the areas painted red indicate failures. The areas painted white indicate that data does exist for the specific angle.

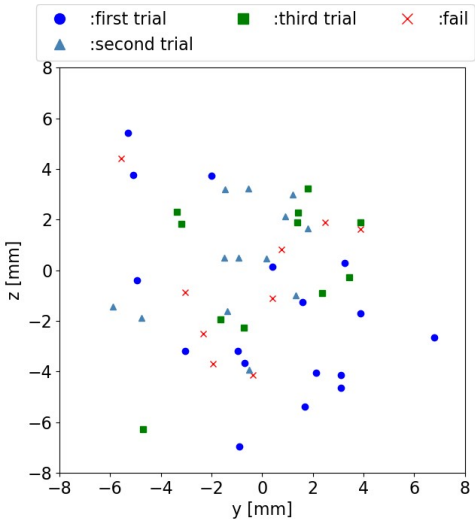

Fig. 16: Experimental results of horizontal peg-in-hole based on the position of the root of the peg. The horizontal axis denotes the position on the y-axis, and the vertical axis denotes the position on the z-axis. Units are in mm. The overall success rate is 82%.

results are 39.5% for 2°, 36.4% for 3°, 36.4% for 4°, and 35.1% for 5°. It should include a larger change angle due to the intention to orient the posture in the opposite direction, and 3° or 4° is acceptable given that there is no significant difference.

The experimental transition is shown in Fig. 13. The CaR method and orientation correction actions were performed twice. If they were unsuccessful, they were considered failures. The direct insertion success was determined by the z-coordinate of the gripper. The experiment was repeated 200 times, during which the peg inclination, position error, success or failure, and execution time were recorded. Additionally, 50 trials of the peg-in-hole experiment were conducted in the horizontal direction.

D. Experimental Results of the Peg-in-Hole Tasks

The experimental results in the vertical direction are shown in Fig. 14 and Fig. 15. The blue circles represent the first CaR, light blue triangles represent the second CaR, and green squares represent the third. The vertical axis represents the position on the x-axis, and the horizontal axis represents the position on the y-axis. These positions were based on the roots of the peg (robot side). This indicates that as the position error increases, the success rate decreases. As shown in Fig. 14, when the position error at the top of the peg was within a circle of radius 2.0 mm, the success rate was 100%. The success rate was 88.9% within a radius of 4.0 mm. After the first orientation correction, the success rate increases to 58.0%. After the second correction, the success rate further improves to 80.0%. As shown in Fig. 15, even in ranges with low success rates, posture adjustments lead to success. These results indicate that the simplified contact position estimation method effectively corrects the orientation and enhances the success rate of the peg-in-hole tasks. The average execution time is 13.52 s with a standard deviation of 7.52 s. For the first, second, and third CaR successes, the average times are 4.21, 12.4, and 21.2 s, respectively. The increased time required for orientation correction was because the peg being withdrawn from the edge, tilted in the correction direction, and pressed again with force f_z. For safety reasons, the operating speed of the robot was decreased, which increased the execution time.

The experimental results in the horizontal direction are shown in Fig. 16. The overall success rate is 82%. The success rate near the center decreased in the horizontal direction compared with that in the vertical direction. This is potentially because gravity does not act in the insertion direction of the peg, and thus it is difficult to insert passively even when it almost overlaps the hole. However, results confirmed that the success rate could be maintained even in the horizontal direction.

IV. Discussion

Table. II compares existing methods with the proposed method. The bottom three rows correspond to the proposed methods, and the top rows correspond to a position error of 2mm, a position error of 4mm, and under all conditions. The results indicate that the proposed method is effective against large position and orientation uncertainties. The success rate of the proposed method is 100% within a radius of 2.0 mm and 88.9% within a radius of 4.0 mm, which indicates a high success rate compared to [12]. The method [16] exhibits an unknown range of position and orientation errors and requires parameter adjustment based on the shape of the peg. Method [19] requires chamfering and can only be used in the vertical direction. In our flexible joint, the arrangement was designed to be usable even in the horizontal direction. When

	hole diameter [mm]	clearance [mm]	position error [mm]	angular error [deg]	chamfer [mm]	ave. time [s]	success rate [%]
[12]	10	0.5	± 2.5	0	0	N/A	84
[16]	50	0.1	N/A	N/A	0	7.20	100
[19]	20	0.1	± 8	0	0.5	5	100
[22]	10	0.036	± 3	0	0.5	37.8	91.8
Our-2mm	16.1	0.1	± 2	± 5	0	7.89	100
Our-4mm			± 4			11.5	88.9
Our-all			± 4			13.5	80

TABLE II: Comparison between this method and conventional methods.

compared to a previous study [22], the speed significantly improved, and the success rate also increased even with similar positional errors, thereby demonstrating the ability to handle angle errors and horizontal peg-in-hole tasks.

V. Conclusion

In this study, we developed and analyzed a hole-search method using flexible joints and peg rotation. The results indicated that robust insertion can be achieved even in the presence of position and orientation errors in the peg in a peg-in-hole assembly. The results indicated that the use of contact position estimation techniques allows posture correction and insertion, even after a failed attempt. The CaR method achieved rapid and simple peg-in-hole operations without relying on high-frequency sensors or servos. In the contact point estimation experiment using a 16mm-diameter-peg, an estimation direction error of 10° was achieved. Even with a simplified contact position estimation method, estimation was sufficient for posture correction. The developed method achieved a success rate of 80.0% in an average time of 13.53 s for peg-in-hole tasks involving a peg diameter of 16 mm and clearance of 0.1 mm, even with position errors ranging from -4.0 to 4.0 mm and an orientation error of 5°. If the position errors were within a radius of 2.0 mm and 4.0 mm, then the success rate was 100% and 88.9%, respectively. Moreover, a success rate of 82.0% was achieved for the horizontal peg-in-hole tasks. A future study aim includes achieving faster and more accurate posture correction by estimating the contact position from force sensors using machine learning techniques.

References

[1] W.-C. Chang and C.-H. Wu, "Automated usb peg-in-hole assembly employing visual servoing," *2017 3rd International Conference on Control, Automation and Robotics (ICCAR)*, pp. 352–355, 2017.

[2] J. Su, H. Qiao, C. Liu, and Z. Ou, "A new insertion strategy for a peg in an unfixed hole of the piston rod assembly," *The International Journal of Advanced Manufacturing Technology*, vol. 59, pp. 1211–1225, 2012.

[3] J. Su, H. Qiao, Z. Ou, and Y. Zhang, "Sensorless insertion strategy for an eccentric peg in a hole of the crankshaft and bearing assembly," *Assembly Automation*, vol. 32, pp. 86–99, 2012.

[4] F. von Drigalski, C. Schlette, M. Rudorfer, N. Correll, J. C. Triyonoputro, W. Wan, T. Tsuji, and T. Watanabe, "Robots assembling machines: learning from the world robot summit 2018 assembly challenge," *Advanced Robotics*, vol. 34, no. 7-8, pp. 408–421, 2020.

[5] W. Newman, Y. Zhao, and Y.-H. Pao, "Interpretation of force and moment signals for compliant peg-in-hole assembly," in *Proceedings 2001 ICRA. IEEE International Conference on Robotics and Automation (Cat. No.01CH37164)*, vol. 1, 2001, pp. 571–576 vol.1.

[6] M. H. Raibert and J. J. Craig, "Hybrid position/force control of manipulators," *Journal of Dynamic Systems, Measurement, and Control*, vol. 103, no. 2, pp. 126–133.

[7] B. Shirinzadeh, Y. Zhong, P. D. W. Tilakaratna, Y. Tian, and M. M. Dalvand, "A hybrid contact state analysis methodology for robotic-based adjustment of cylindrical pair," *The International Journal of Advanced Manufacturing Technology*, vol. 52, pp. 329–342, 2011.

[8] Y.-L. Kim, H.-C. Song, and J.-B. Song, "Hole detection algorithm for chamferless square peg-in-hole based on shape recognition using f/t sensor," *International Journal of Precision Engineering and Manufacturing*, vol. 15, pp. 425 – 432, 2014.

[9] F. Chaumette and S. A. Hutchinson, "Visual servo control. i. basic approaches," *IEEE Robotics & Automation Magazine*, vol. 13, pp. 82–90, 2006.

[10] N. Zhu, W.-F. Xie, and H. Shen, "Position-based visual servoing of a 6-rss parallel robot using adaptive sliding mode control." *ISA transactions*, 2023.

[11] J. Wang, A. Liu, X. Tao, and H. Cho, "Microassembly of micropeg and -hole using uncalibrated visual servoing method," *Precision Engineering-journal of The International Societies for Precision Engineering and Nanotechnology*, vol. 32, pp. 173–181, 2008.

[12] S. Kozlovsky, E. Newman, and M. Zacksenhouse, "Reinforcement learning of impedance policies for peg-in-hole tasks: Role of asymmetric matrices," *IEEE Robotics and Automation Letters*, vol. 7, pp. 10 898–10 905, 2022.

[13] C. C. Beltran-Hernandez, D. Petit, I. G. Ramirez-Alpizar, and K. Harada, "Variable compliance control for robotic peg-in-hole assembly: A deep reinforcement learning approach," *Applied Sciences*, vol. 10, no. 19, p. 6923, 2020.

[14] Y. Shen, Q. Jia, R. Wang, Z. Huang, and G. Chen, "Learning-based visual servoing for high-precision peg-in-hole assembly," *Actuators*, 2023.

[15] J. Su, R. Li, H. Qiao, J. Xu, Q. Ai, and J. Zhu, "Study on dual peg-in-hole insertion using of constraints formed in the environment," *Ind. Robot*, vol. 44, pp. 730–740, 2017.

[16] H. Park, J. Park, D.-H. Lee, J.-H. Park, and J.-H. Bae, "Compliant peg-in-hole assembly using partial spiral force trajectory with tilted peg posture," *IEEE Robotics and Automation Letters*, vol. 5, pp. 4447–4454, 2020.

[17] H. Dallali, P. Kormushev, N. G. Tsagarakis, and D. G. Caldwell, "Can active impedance protect robots from landing impact?" in *2014 IEEE-RAS International Conference on Humanoid Robots*, 2014, pp. 1022–1027.

[18] W. Haskiya, K. Maycock, and J. Knight, "A passive compliant wrist for chamferless peg-in-hole assembly operation from vertical and horizontal directions," *Proceedings of the Institution of Mechanical Engineers, Part B: Journal of Engineering Manufacture*, vol. 212, pp. 473 – 478, 1998.

[19] Q. Zhang, Z. Hu, W. Wan, and K. Harada, "Compliant peg-in-hole assembly using a very soft wrist," *IEEE Robotics and Automation Letters*, vol. 9, pp. 17–24, 2024.

[20] M. Tennomi, A. Okamura, Y. Nakamura, T. Abe, S. Wakamatsu, S. Tajima, T. Nishimura, Y. Hirai, T. Sawada, N. Ichikawa, T. Tsuji, K. Yamazaki, Y. Suzuki, and T. Watanabe, "Development of assembly system with quick and low-cost installation," *Advanced Robotics*, vol. 34, pp. 531 – 545, 2020.

[21] T. Nishimura, Y. Suzuki, T. Tsuji, and T. Watanabe, "Peg-in-hole under state uncertainties via a passive wrist joint with push-activate-rotation function," in *2017 IEEE-RAS 17th International Conference on Humanoid Robotics (Humanoids)*. IEEE, 2017, pp. 67–74.

[22] M. Ueda, T. Tsuji, T. Hiramitsu, H. Seki, T. Nishimura, Y. Suzuki, and T. Watanabe, "Tight clearance peg-in-hole motion planner using gripper with flexible joint and differential infinity rotatable function of palm," *IEEE/SICE International Symposium on System Integrations (SII)*, 2025.